Charge-state measurements of backscattered ions from Au films

D.-E. Arafah, J. D. Meyer,* H. Sharabati, and A. Mahmoud
Physics Department, University of Jordan, Amman, Jordan
(Received 28 September 1988)

A small electrostatic accelerator (65 kV) was built as a postaccelerator for measuring the charge-state fractions of ions backscattered from solid or gas targets. A new method is described in which the charge-state fractions of ^{3}He, ^{4}He, ^{12}C, ^{14}N, and ^{16}O ions backscattered from gold films are determined simultaneously. The added features in this work are the facts that the method can be efficiently used for low-energy incident ions and that spectra could be measured, compared, and analyzed by minimizing uncertainties inherent in experimental parameters. The energy dependence of the charge-state fractions of ^{3}He, ^{4}He, and ^{12}C ions are measured between 3 MeV and 150 keV. The ^{12}C charge-state-fraction data nicely fit the Gaussian model but none of the χ^2 models. The mean ion charge i_m and the standard deviation s are also measured. Preliminary measurements of the dependence of the charge-state fractions on target thickness are also discussed.

I. INTRODUCTION

Rutherford-backscattering spectrometry (RBS) has proved to be a powerful and versatile technique for surface and near-surface analysis of solids.[1] The method has been applied extensively to the analysis of metals and semiconductors, but relatively few examples have been cited for dielectric materials. In all applications, information is conveyed through the energy spectra which are measured using either a surface-barrier detector (SBD), an electrostatic analyzer (ESA), or position-sensitive channel plates.

The knowledge of the charge states of ions backscattered from solid surfaces is crucial in understanding energy-loss processes. However, variation in the charge states of backscattered ions are known to markedly influence the measured backscattering yield.[2] The literature on the charge states of backscattered ions from solid surfaces is numerous (e.g., Refs. 3–6). The subject has been thoroughly surveyed by Betz[7] and Datz.[8] More recent data include works by Lennard *et al.*[9] and Robinet.[10] However, simultaneous measurements of all charge states in one run is not frequent.[11] In most of the measurements carried out, light or heavy ions passing through thin films of different materials or traversing gaseous media, covering a limited energy range, were used.[12–14] Charge neutralization of low-energy helium ions scattered from silicon surfaces was also reported by Haight *et al.*[15]

Several conclusions can be drawn from earlier works. First, the equilibrium charge states primarily depend on the ion velocity. Second, the equilibrium charge-state distribution can be fitted by the χ^2, reduced χ^2, or Gaussian statistical models depending on the ion species and their velocities. Third, the charge-state fractions are insensitive to the type of target material used, but show a weak dependence on the depth at which scattering events occur. Fourth, the ion fractions can be predicted if the mean charge i_m, and the standard deviation s of the distribution are precisely determined. Finally, channeling plays some role in the distribution of ion fractions of backscattered particles.

In this paper, the charge-state fractions of ^{3}He, ^{4}He, ^{12}C, ^{14}N, and ^{16}O ions backscattered from gold surfaces are measured between 3 MeV and 150 keV. In addition, the charge-state distributions as function of incident energy are also determined. The new approach followed throughout this experimental work is that all charge-state fractions are measured simultaneously in one run. Hence, uncertainties inherent in the more traditional methods are minimized.

II. EXPERIMENT

Monoenergetic ion beams with relatively low-energy spread (less than 500 eV) are produced by the 4.75-MeV University of Jordan Van de Graaff accelerator (JOVAC). Light ions with energies ranging from 3 MeV down to 150 keV were used. The highest energies for the heavier monoatomic ions (e.g., $^{12}C^+$, $^{14}N^+$, and $^{16}O^+$) are limited by the bending power of the switching magnet. The focused and well-collimated beam is directed into a 4-m beam line and passes through a pair of collimators. The final beam diameter before entering the scattering chamber can be adjusted by the second, micrometer-driven aperture.

The charge-state-fraction measurements were carried out using a postaccelerator which was built locally, see Fig. 1. The scattering chamber linked to the accelerator is equipped to measure the charge-state fractions resulting from ions, and gaseous- or solid-target interactions. The applied voltage to the accelerator system is distributed over seven stages in the main column. The column current at 50 keV is 25 nA. A preacceleration column of three stages is located inside the scattering chamber and can be biased up to 3 kV. This preacceleration column was not used during the charge-state-fraction measurements resulting from solid targets. The diameter of the entrance aperture in front of the detector is 1 cm, whereas the overall distance from target to detector is 90

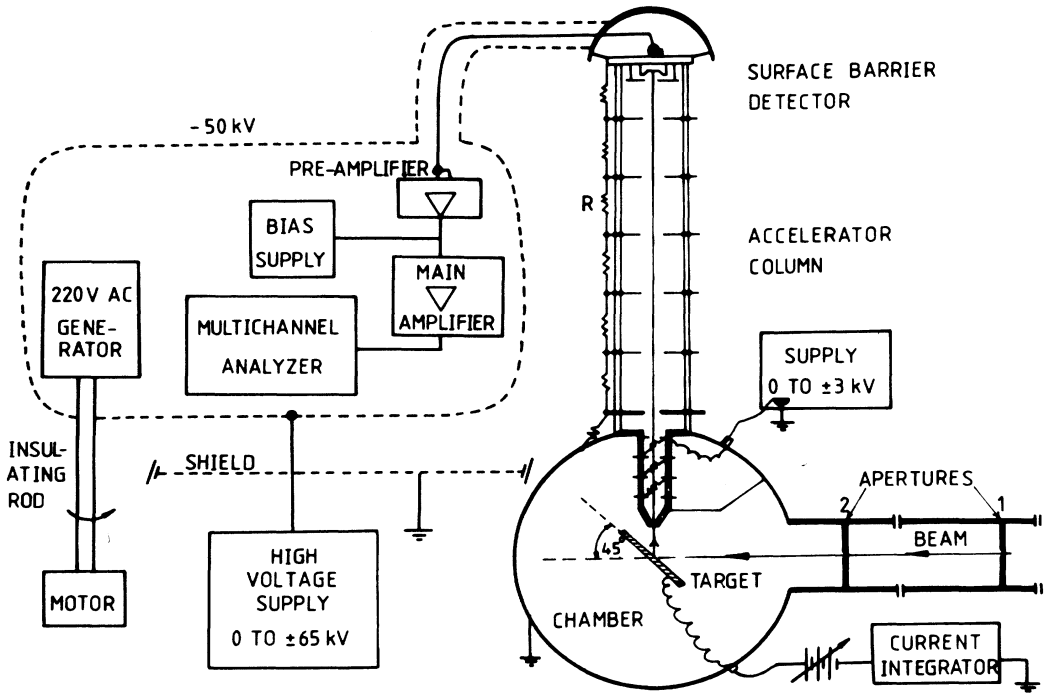

FIG. 1. Block diagram showing the experimental setup and the 65-keV postacceleration built as a charge-state separator of backscattered ions.

cm. The angle of detection is 90° and the target is placed at an angle of 45° with respect to the beam direction. The conventional electronics needed for backscattering measurements[1] with a SBD and a multichannel analyzer (MCA) were all at negative potential relative to ground (cf. Fig. 1). The bias supply to all electronics is furnished through a motor-generator combination. The high voltage supplied to the setup is powered by a 65-kV FUG power-supply unit (HCN 140-6500) which allows for reversing the polarity of the voltage. The operating pressure inside both the chamber and the accelerator column was typically 5×10^{-6} Torr. There was, however, no observed dependence of the charge-state fractions on the pressure inside the target chamber and the accelerator column up to a pressure of about 10^{-4} Torr.

The charge-state analysis of backscattered ions from solid targets is a straightforward process. The kinematic behavior of the backscattered ions is given by the well-known RBS technique.[1] The surface-barrier detector analyzes the energy distribution typically observed for ions backscattered from thin films. With an additional electrostatic energy of, e.g., -50 keV between the target and SBD, the reflected ions will gain multiples of this acceleration energy depending on their ionic charge state n (i.e., $n\times50$ keV). This, however, allows all charge-state fractions ranging from positive to negative values to be collected and measured simultaneously in one experimental run. The statistical error can be improved by increasing the time of collection. However, typical measuring times for obtaining reasonable statistics are of the order of 1 h or less.

In the present work, only solid targets are investigated. Thin layers of gold films ranging in thickness between 45 and 110 Å were prepared by vacuum evaporation on silicon-wafer substrates. One should notice that evaporated thin gold films, of thicknesses below ≤ 100 Å, may result in an uneven texture of gold.[16] Gold, however, was chosen to minimize the overlap between ions reflected from the backing material and the signal from the target, especially at the lowest energies used. The thickness of the target was determined using a calibrated quartz-crystal monitor. Typical energy spectra obtained are shown in Figs. 2 and 3 for 2-MeV $^4He^+$ and 1-MeV $^{12}C^+$, respectively, backscattered from 45-Å gold films. The statistical error associated with the number of counts in the gold peak was always maintained well below 1%.

III. DATA ANALYSIS AND DISCUSSION

Data acquisition and analysis proceed in two steps. First, the accumulation of an RBS energy spectrum without postacceleration is carried out. The resulting spectrum is then fitted by an analytical function $f(E)$. An exponential fit was, in most cases, used for both the low- and high-energy tails of the spectrum as well as for regions around the maximum of the profile. The obtained function conveys two important pieces of information. One is the channel number (or energy) corresponding to the peak of the distribution (i.e., the reference or relative zero channel number corresponding to all charge-state fractions) and the other is the shape (in particular, the width) of the distribution profile. Second, the

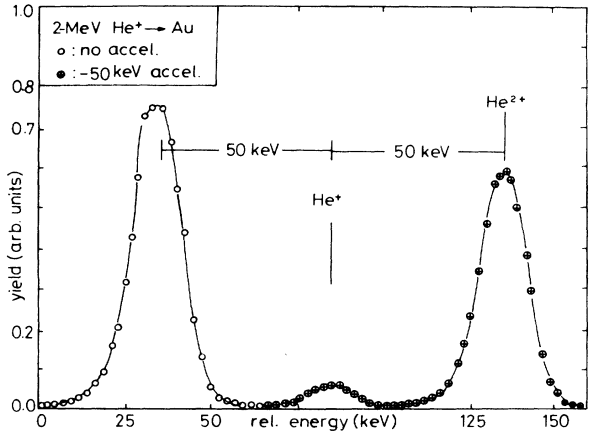

FIG. 2. RBS energy spectra of 2-MeV ^{4}He ions backscattered from 45-Å Au film. Spectra are labeled as with (⊕) and without (○) postacceleration. The latter clearly shows the separation of both ^{4}He isotopes.

accumulation of a RBS energy spectrum for a fixed postacceleration voltage V (e.g., $V=-50$ kV) is then carried out. The resulting spectrum is now fitted by an analytical function which is the sum of the weighted functions $f(E+nqV)$ according to the following equation:

$$\left[\sum_n C_n f(E+nqV)-Y(E)\right]^2=\text{minimum}\ ,$$

where again $f(E)$ is the fitted analytical function without postacceleration voltage, E is the energy spanned over the RBS energy spectrum as obtained without postacceleration, and C_n are fitting coefficients for the n-fold charge-state-fractional contribution accelerated by energy nqV. $Y(E)$ is the yield corresponding to a RBS energy spectrum with the fixed postacceleration voltage V. The results of this procedure are shown in Fig. 2 for ^{4}He$^+$ and Figs. 3 and 4 for ^{12}C$^+$.

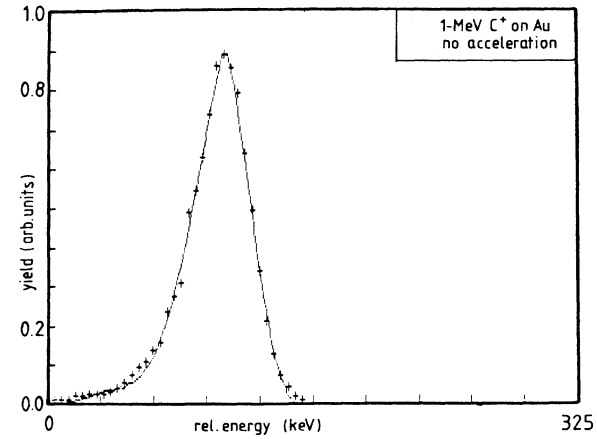

FIG. 3. RBS energy spectrum of 1-MeV ^{12}C ions backscattered from 45-Å Au film without postacceleration. The solid curve is the least-squares fit to the obtained data.

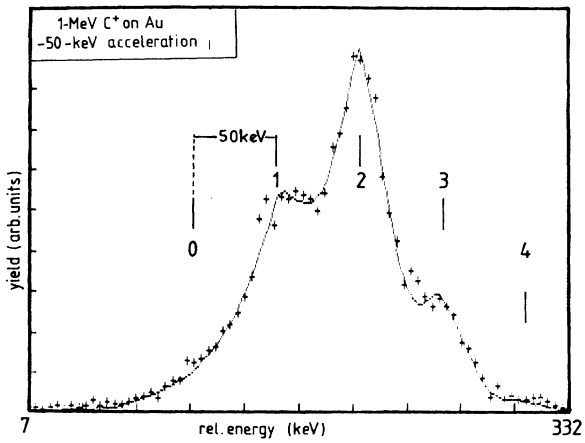

FIG. 4. Same as Fig. 3, but with −50-keV postacceleration voltage. The peaks are labeled according to their charge state.

Several conclusions can be drawn by referring to, e.g., Fig. 2. First, the −50-kV postacceleration voltage separates the ^{4}He$^+$ from ^{4}He^{2+} charge-state fractions of helium. Second, the energy difference between the peaks for all charge states (i.e., peak in the spectrum without postacceleration) and the separated peaks corresponding to ^{4}He$^+$ and ^{4}He^{2+} is always 50 keV. Third, for the same charge collected on the sample, the integrated yield for the spectra with and without postacceleration is the same. It should, however, be emphasized that the spectra presented in Figs. 3 and 4 are not normalized to the same incident charge on the target.

For thin targets (e.g., 45 Å) good fits were obtained with the original function without postacceleration. In particular, both the half-width of the function $f(E)$ and the location of the relative zero energy, or reference channel number, need not be modified. Some corrections which were eventually necessary for thicker targets will be discussed later.

Figure 5 shows the resulting charge-state fractions C_n for ^{3}He$^+$ and for ^{4}He$^+$ backscattered from thin Au films.

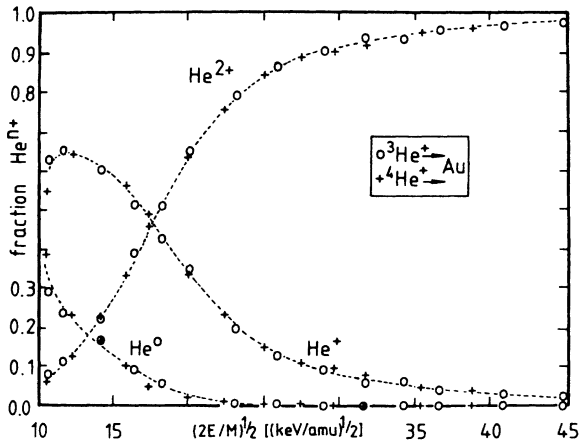

FIG. 5. Charge-state fractions of backscattered ^{3}He and ^{4}He as a function of the incident-ion velocity.

The abscissa represents the ion velocity measured in $(\text{keV/amu})^{1/2}$. It can be clearly seen that for the energy range studied (from 3 MeV down to 250 keV), no significant differences in the charge-state fractions of both helium isotopes are observed for the same incoming ion's velocity. In addition, near the lower-energy edge of the scale (i.e., below 250 keV) the peaks of the neutral and single-charged ^{3}He ions overlap with counts resulting from the charge-state fractions of the backing material, i.e., silicon. Background corrections for these peaks constitute a difficulty, since the charge-ion fractions reaching the detector from the backing substrate will also be shifted towards higher energies as a result of the postacceleration. It should be noted that when the postacceleration voltage is inverted to positive values, the same charged-ion fractions are obtained for the same velocity of incoming ions, as in the case of negative values. In addition, it must be emphasized that for the same accumulated charge, the integrated yield with and without postacceleration is the same. These facts exclude any significant influence of focusing of the beam when the accelerated voltage is applied. Hence, insignificant effects on the measured charge-state distributions are observed. If, however, such focusing effects are present, then serious consequences could affect the accuracy of the experiment since the accelerating column would act as a series of lenses between the scattering centers and the detector system when using the accelerated configuration. The results presented for helium in Fig. 5 are in excellent agreement with those obtained by Dissanaike[12] using an experimental setup in which the measured charge-state fractions were recorded by an ESA after passing through thin Au foils. The fact that the calculated distributions reproduce the experimental distributions well firstly tests the setup used, secondly, emphasizes the point that the method can also be used for low energy ions, and thirdly confirms that reliable results are obtained with minimum inherent uncertainties due to experimental parameters.

The data analysis for the other monoatomic ion-beam species, i.e., ^{12}C, ^{14}N, and ^{16}O, was carried out in the same manner as for helium. The energy dependence of the charge-state fractions for, e.g., ^{12}C ions backscattered from 45-Å thin Au films, is given in Table I and Fig. 6. The solid curves in Fig. 6 were calculated assuming a Gaussian distribution $G(i)$ for the charge-state fractions at a given energy (or velocity),[6] namely

$$G(i)=\frac{1}{(2\pi s^2)^{1/2}}\exp\{-\tfrac{1}{2}[(i-i_m)^2/s^2]\}\ ,$$

where i_m is the mean ion charge of the distribution and s is the standard deviation. Both i_m and s were calculated from each set of the charge-fraction data at one particular energy by solving the above equation. The mean values of i_m and s, plotted against the ion's velocity, are presented in Figs. 7 and 8, respectively. The solid lines represent a linear and a quadratic fit to both i_m (cf. Fig. 7) values, respectively. The dotted line in Fig. 7 gives, on the other hand, the effective charge i_{eff} calculated according to $i_{\text{eff}}=\sum_n C_n n$ for each set of charge-state fractions. The fits to both i_m and s values were used to obtain the curves in Fig. 6. Neither the χ^2 nor the reduced χ^2 fits give a good approximation in comparison to the Gaussian fit shown in Fig. 6. However, the slopes of the lines shown in Fig. 7 give 0.157 and 0.163 $(\text{amu/keV})^{1/2}$ for i_{eff} and i_m, respectively. The variance of the data is within the width of the plus symbols for all i_m values obtained. When the calculated charge-state distribution function $G(i)$ is extrapolated to $i=-1$, an expected fraction of 0.04 (0.016) at 200 (400) keV is obtained. Experimentally, such a charge state was not possible to detect since the backscattered ions from the silicon substrate overlap with both of negative-charge-state carbon peaks. For energies greater than 600 keV, no negative-single-charge states could be detected.

The charge-state fractions of ^{12}C, ^{14}N, and ^{16}O are presented in Table I. It can be clearly seen that for both ^{14}N and ^{16}O the mean charge i_m is larger than the corresponding values for ^{12}C. Also, the lower-charge-state fractions (i.e., q^0 and q^{1+}) for ^{14}N and ^{16}O are smaller, at

TABLE I. Charge-state fractions for ^{12}C, ^{14}N, and ^{16}O ions backscattered from 45-Å gold films.

Ion	Energy (keV)	Velocity $(\text{keV/amu})^{1/2}$	Fraction (%) q^0	q^{1+}	q^{2+}	q^{3+}	q^{4+}	i_{eff}	i_m	s
$^{12}C^+$	200	05.77	37.7	51.0	10.8	0.5	0.0	0.74	0.66	0.749
	400	08.16	22.1	50.5	24.6	2.8	0.0	1.08	1.03	0.812
	600	10.00	11.3	46.0	37.0	5.2	0.5	1.38	1.37	0.804
	800	11.55	5.5	37.1	46.6	9.9	0.9	1.64	1.63	0.809
	1000	12.91	5.0	28.1	50.2	15.4	1.3	1.80	1.81	0.813
	1200	14.14	3.1	20.7	49.7	23.2	3.2	2.03	2.04	0.846
	1400	15.28	1.7	15.6	47.4	30.5	4.8	2.21	2.21	0.843
	1600	16.33	0.5	11.3	44.5	36.6	7.1	2.39	2.38	0.803
	1800	17.32	0.0	7.3	39.1	44.8	8.9	2.55	2.57	0.764
	2000	18.26	0.0	5.4	34.9	47.2	12.5	2.67	2.68	0.793
$^{14}N^+$	800	10.69	4.4	28.2	46.5	18.4	2.6	1.86	1.88	0.872
	1500	14.64	1.1	9.3	38.1	44.1	7.5	2.48	2.42	0.885
$^{16}O^+$	350	06.61	21.0	49.5	25.3	4.0	0.2	1.13	1.07	0.885

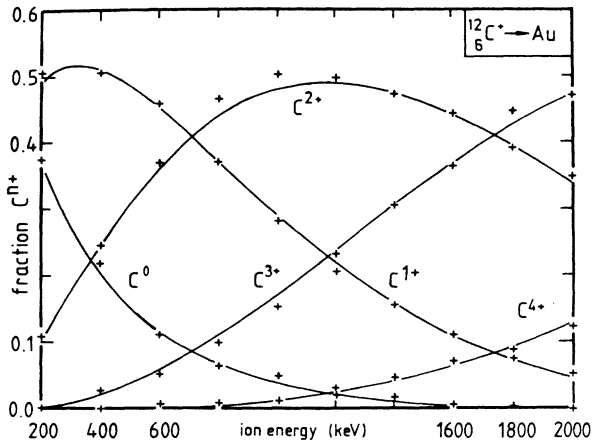

FIG. 6. Charge-state fractions of backscattered ^{12}C from 45-Å Au film as a function of the incident-ion energy. The solid curves are calculated using the Gaussian model with the mean charge i_m and the standard deviation s, obtained from Figs. 7 and 8, respectively.

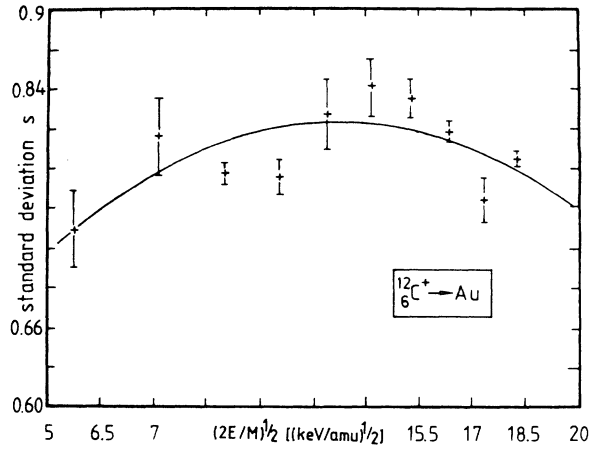

FIG. 8. The standard deviation s as a function of the ion velocity calculated from the data of Fig. 6. The error bars represent the variance of the standard deviation.

the same velocity, than the corresponding fractions for ^{12}C. On the other hand, this behavior is reversed for the higher-charge-state fractions, i.e., q^{3+} and q^{4+} are larger for ^{16}O and ^{14}N than for ^{12}C. The slopes of i_m and i_{eff} as a function of ion velocity are 0.137 and 0.157 $(\text{amu/keV})^{1/2}$, respectively. An expected negative ^{16}O fraction of about 4% was experimentally not detected due to signal overlap from the silicon substrate.

The analysis carried out using thicker films (e.g., 110 Å) revealed that the full width of a RBS energy spectrum without postacceleration is nearly 30% wider than a corresponding spectrum obtained with postacceleration. In addition, the lower- (higher-) charge-state fractions obtained are increased (decreased) against the fractions of thinner films for the same ion energy (or velocity). Furthermore, the mean ion charge is reduced, whereas the standard deviation is increased against thinner films under the same conditions. These two observations, taken together, lead to a physical impossibility, i.e., ingoing from charge $1+$ to charge $q+$ one does not usually pass through a charge higher than $q+$. In this respect, one may infer this to different causes, e.g., uniformity of the deposited Au layers, for example, see Ref. 16. The preliminary results obtained for the thicker films, therefore, merely point out that the charge-state fractions obtained for 45-Å films represent the nonequilibrium fractions since there are differences in the distributions obtained. The question at which thickness the equilibrium fractions are reached can be answered if the thickness and energy dependence of the charge-state fractions of backscattered ions is measured. Experiments on the thickness dependence of the charge-state fractions are, however, in progress.

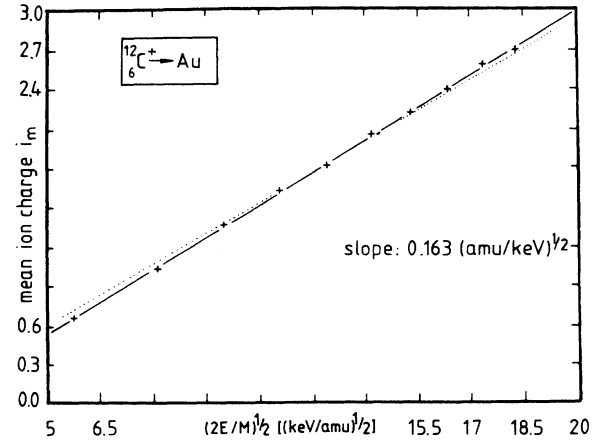

FIG. 7. Mean ion charge (the solid line) of ^{12}C as a function of the ion velocity calculated from Fig. 6. The dotted line gives the effective charge with a slope of 0.157 $(\text{amu/keV})^{1/2}$.

As an interesting result of this study, it turned out that the charge-state fractions as obtained from the 45-Å thin-Au-film data represent the nonequilibrium distribution. On the other hand, the distribution for these fractions is still fitted by the Gaussian model, which is based on the assumption of equilibrium distributions. Therefore, it becomes necessary to investigate at which thickness the statistical model breaks down. This is very important for understanding the mechanism of charge-transfer processes of backscattered ions. For this purpose, experiments on the thickness dependence of the charge-state fractions are under preparation. The method has also emphasized the fact that it can be used for low-energy ions; however, one major problem during the course of this experiment was due to the undesired influence of the backing material. A low-atomic-number metal or semimetal should be used in order to avoid matrix-signal overlap. The previous problem constitutes the major uncertainty in our measurements. All other sources of errors, e.g., energy spread and detector and system resolutions, were successfully eliminated by carrying out deconvolution procedures on the experimental data. On the other hand, the accuracy of the calculated

distributions is somewhat difficult to assess. However, based on the data collected which involve a minimization procedure by following a statistical approach, the error in the calculations is generally below 2% but increases to about 4% at lower energies. Finally, the new feature of the spectrometer described for detecting all charge states simultaneously in one run contributes to the accuracy and minimization of inherent uncertainties in experimental parameters.

IV. CONCLUSIONS

The charge-state-fraction data of ^{3}He, ^{4}He, ^{12}C, ^{14}N, and ^{16}O ions backscattered from Au films were measured for the energy range between 3 MeV and 150 keV. The charge-state distributions as a function of the incident ion energies were also determined. The mean ion charge and the standard deviation were calculated. The charge-state data for helium reveal identical distributions for both helium isotopes. The nonequilibrium data of ^{12}C were fitted nicely by the Gaussian model, which is based on equilibrium distribution. The preliminary results obtained with thicker targets suggest that a more concrete investigation of the thickness dependence of the charge-state fractions is needed, in order to reveal the critical thickness at which the statistical model breaks down. The method has emphasized the point that it can also be used for low-energy ions. Finally, the capability of the new method described in successfully unfolding all charge states in one experimental run adds to the reliability of the obtained results by minimizing uncertainties inherent in the experimental parameters.

ACKNOWLEDGMENTS

The immense help received from the Physics Mechanical and Electronics workshops in building the accelerator system is greatly appreciated. Special thanks are due to Dr. R. Boulus for encouragements and fruitful discussions during the building of the postacceleration system.

---

*Permanent address: Institut für Kernphysik, August Euler Strasse 6, Frankfurt, D-6000 Frankfurt am Main, Federal Republic of Germany.

[1]W. K. Chu, J. W. Mayer, and M.-A. Nicolet, *Backscattering Spectrometry* (Academic, New York, 1978).

[2]T. M. Buck, Y.-S. Chen, G. H. Wheatley, and W. F. Van der Weg, Surf. Sci. **47**, 244 (1975).

[3]T. M. Buck, G. H. Wheatley, and L. C. Feldman, Surf. Sci. **35**, 345 (1973).

[4]P. Meischner and H. Verbeek, J. Nucl. Mater. **53**, 276 (1974).

[5]W. Eckstein, H. Verbeek, and S. Datz, Appl. Phys. Lett. **27**, 527 (1975).

[6]W. Eckstein, V. A. Molchanov, and H. Verbeek, Nucl. Instrum. Methods **149**, 599 (1978).

[7]H. Betz, Rev. Mod. Phys. **44**, 465 (1972).

[8]S. Datz, Nucl. Instrum. Methods **132**, 7 (1976).

[9]W. N. Lennard, D. Philips, and D. A. Walker, Nucl. Instrum. Methods **179**, 413 (1981).

[10]Y. B. Robinet, Phys. Rev. A **26**, 62 (1982).

[11]S. Datz, H. O. Lutz, L. B. Bridwell, C. D. Moak, H. D. Betz, and L. D. Ellsworth, Phys. Rev. A **2**, 430 (1970).

[12]G. A. Dissanaike, Philos. Mag. **44**, 1051 (1954).

[13]B. L. Cardon, H. Oona, and J. A. Leavitt, Phys. Rev. A **21**, 515 (1980).

[14]R. M. Tromp, R. G. Smeenk, and F. W. Saris, Surf. Sci. **104**, 13 (1981).

[15]R. Haight, L. C. Feldman, T. M. Buck, and W. G. Gibson, Nucl. Instrum. Methods B **2**, 501 (1984).

[16]C. D. Moak, T. W. T. Dabbs, and W. W. Walker, Rev. Sci. Instrum. **37**, 1131 (1966).